LETTERS

A fast, robust and tunable synthetic gene oscillator

Jesse Stricker[1]*, Scott Cookson[1]*, Matthew R. Bennett[1,2]*, William H. Mather[1], Lev S. Tsimring[2] & Jeff Hasty[1,2]

One defining goal of synthetic biology is the development of engineering-based approaches that enable the construction of gene-regulatory networks according to 'design specifications' generated from computational modelling[1–6]. This approach provides a systematic framework for exploring how a given regulatory network generates a particular phenotypic behaviour. Several fundamental gene circuits have been developed using this approach, including toggle switches[7] and oscillators[8–10], and these have been applied in new contexts such as triggered biofilm development[11] and cellular population control[12]. Here we describe an engineered genetic oscillator in *Escherichia coli* that is fast, robust and persistent, with tunable oscillatory periods as fast as 13 min. The oscillator was designed using a previously modelled network architecture comprising linked positive and negative feedback loops[1,13]. Using a microfluidic platform tailored for single-cell microscopy, we precisely control environmental conditions and monitor oscillations in individual cells through multiple cycles. Experiments reveal remarkable robustness and persistence of oscillations in the designed circuit; almost every cell exhibited large-amplitude fluorescence oscillations throughout observation runs. The oscillatory period can be tuned by altering inducer levels, temperature and the media source. Computational modelling demonstrates that the key design principle for constructing a robust oscillator is a time delay in the negative feedback loop, which can mechanistically arise from the cascade of cellular processes involved in forming a functional transcription factor. The positive feedback loop increases the robustness of the oscillations and allows for greater tunability. Examination of our refined model suggested the existence of a simplified oscillator design without positive feedback, and we construct an oscillator strain confirming this computational prediction.

The synthetic gene oscillator is based on a previously reported theoretical design[1] and was constructed using *E. coli* components (Fig. 1a). The hybrid promoter ($p_{lac/ara-1}$; ref. 14) is composed of the activation operator site from the *araBAD* promoter placed in its normal location relative to the transcription start site, and repression operator sites from the *lacZYA* promoter placed both upstream and immediately downstream of the transcription start site. It is activated by the AraC protein in the presence of arabinose and repressed by the LacI protein in the absence of isopropyl β-D-1-thiogalactopyranoside (IPTG). We placed the *araC*, *lacI* and *yemGFP* (monomeric yeast-enhanced green fluorescent protein) genes under the control of three identical copies of $p_{lac/ara-1}$ to form three co-regulated transcription modules (Supplementary Information). Hence, activation of the promoters by the addition of arabinose and IPTG to the medium results in transcription of each component of the circuit, and increased production of AraC in the presence of arabinose results in a positive feedback loop that increases promoter activity. However, the concurrent increase in production of LacI results in a linked negative feedback loop that decreases promoter activity, and the differential activity of the two feedback loops can drive oscillatory behaviour[1,13].

The oscillator cells (denoted JS011) exhibited ubiquitous fluorescence oscillations over the entire run time of each experiment (at least 4 h). For example, at 0.7% arabinose and 2 mM IPTG, more

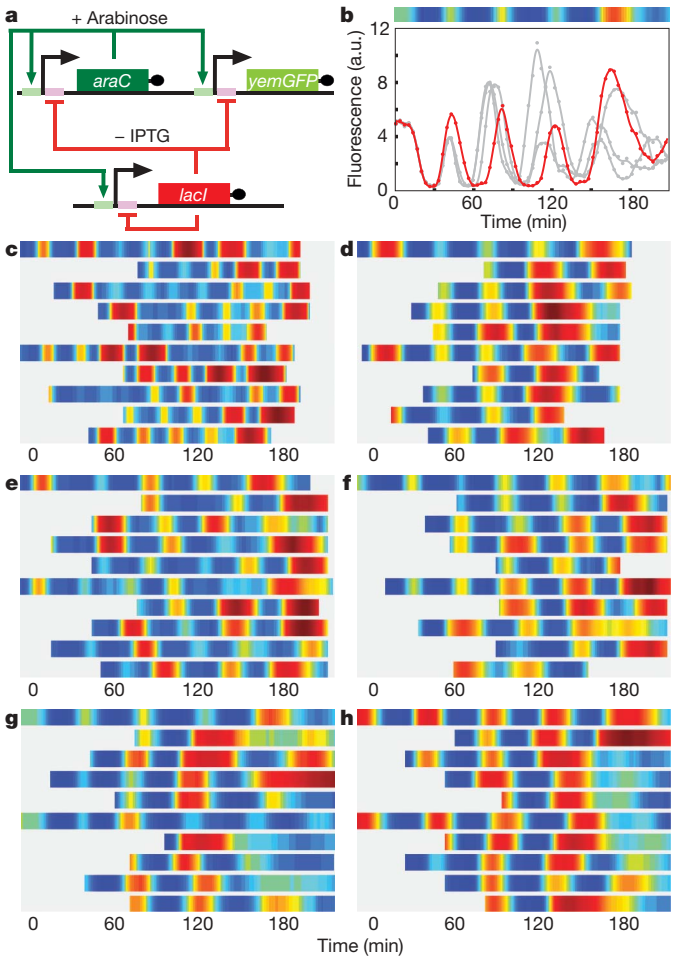

Figure 1 | Oscillations in the dual-feedback circuit. a, Network diagram of the dual-feedback oscillator. A hybrid promoter $p_{lac/ara-1}$ drives transcription of *araC* and *lacI*, forming positive and negative feedback loops. **b**, Single-cell fluorescence trajectories induced with 0.7% arabinose and 2 mM IPTG. Points represent experimental fluorescence values, and solid curves are smoothed by a Savitsky–Golay filter (for unsmoothed trajectories, see Supplementary Fig. 3). The trajectory in red corresponds to the density map above the graph. Density maps for trajectories in grey are shown in **g**. a.u., arbitrary units. **c**–**h**, Single-cell density map trajectories for various IPTG conditions (**c**, 0 mM IPTG; **d**, 0.25 mM; **e**, 0.5 mM; **f**, 1 mM; **g**, 2 mM; **h**, 5 mM).

[1]Department of Bioengineering, University of California, San Diego, La Jolla, California 92093, USA. [2]Institute for Nonlinear Science, University of California, San Diego, La Jolla, California 92093, USA.
*These authors contributed equally to this work.

than 99% of the cells showed oscillations with a period of approximately 40 min (Fig. 1b, g, Supplementary Table 1 and Supplementary Movie 1). The highly dynamic nature of the oscillator components is shown by the rapid decay of green fluorescent protein (GFP) signal, which drops from peak to trough in less than 10 min (Fig. 1b). The oscillatory phase was heritable between daughter cells, which resulted in synchronized oscillations in areas of the microcolony derived from a common cell. This synchrony was limited to a few periods, presumably owing to oscillatory phase diffusion. We used a microfluidic device with a laminar boundary switch upstream of the growth chamber to investigate the initiation of synchronized oscillations (Supplementary Fig. 2c, d). Cells grown in the absence of inducer initiated oscillations in a synchronous manner on the addition of inducer (Supplementary Movie 10), which suggested the possibility of using flow cytometry to characterize the oscillator further. Flow cytometry of samples continuously collected from a culture in logarithmic growth that had been induced with 0.7% arabinose and 2 mM IPTG showed oscillations in mean cell fluorescence (Supplementary Fig. 8). Induction of oscillation was very quick (less than 5 min) and initially well-synchronized. The amplitude of these bulk oscillations decayed as the experiment progressed, as expected from the desynchronization of individual cells in the colony (Supplementary Information). However, the period obtained from the flow cytometry method (green data points in all figures) compared favourably to that obtained from single cells using microscopy (red data points in all figures).

The oscillator was extremely robust over an extensive range of inducer conditions and temperatures. At 0.7% arabinose and 37 °C, almost every observed cell oscillated (Supplementary Table 1) at all IPTG concentrations examined (Fig. 1b–h and Supplementary Movies 1–8). Varying the IPTG concentration allowed for the tuning of the oscillator period (Fig. 2a), particularly at low IPTG concentrations. The period decreased at high IPTG concentrations, and subsequent characterization of the promoter revealed that this non-monotonic behaviour is probably caused by IPTG interference with AraC activation[15] (Supplementary Information). The cell doubling time on the microfluidic device remained largely steady between experiments, ranging from 22.3 min to 27.6 min at 37 °C and showing little correlation to IPTG concentration ($R^2 = 0.132$). Individual cell fluorescence trajectories showed a gradual increase in oscillatory period as the cells were imaged on the microfluidic device (Supplementary Fig. 4). This increase was not seen in doubling times, implying that the cells were not experiencing nutritional difficulties or environmental stress that might cause an alteration in oscillator behaviour.

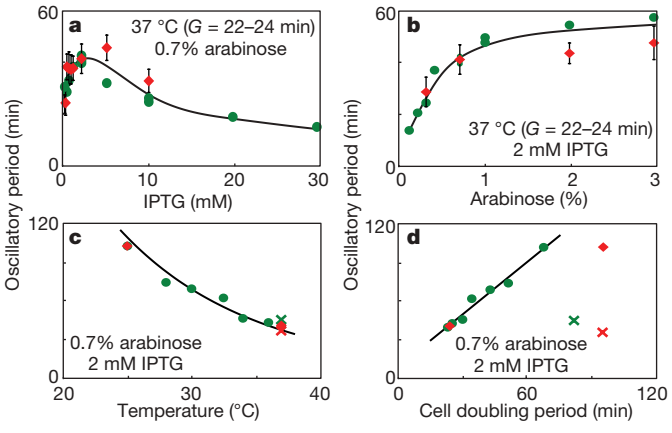

Figure 2 | Robust oscillations. **a–c**, Oscillatory periods on transects with 0.7% arabinose and varying IPTG (**a**), 2 mM IPTG and varying arabinose (**b**), or 0.7% arabinose, 2 mM IPTG, and varying temperature (**c**). Mean periods from single-cell microscopy (red diamonds, mean ± s.d.) or flow cytometry (green circles) are shown. Black curves are trend lines in **a** and **b**, or represent the theoretical prediction based on reference values at 30 °C in **c** (see Supplementary Information). Samples grown in minimal medium rather than LB are indicated by crosses. *G* represents the cell doubling period. **d**, Oscillatory period and cell division time increase monotonically as the growth temperature decreases. Symbols are as described above, and the black line is a linear regression of samples grown in LB.

To explore further the robustness of the oscillator, we investigated the effect of varying arabinose, temperature and the media source. At a fixed value of 2 mM IPTG and at 37 °C, the oscillatory period can be tuned from 13 min to 58 min by varying the arabinose level from 0.1% to 3.0% (Fig. 2b). Cells grown in the absence of arabinose did not express measurable levels of GFP in single-cell microscopy or flow cytometry experiments, and high levels of arabinose seemed to saturate the system. We observed sustained oscillations at a range of temperatures from 25 °C to 37 °C, with a decreasing period as a function of temperature (Fig. 2c). The cell doubling time also decreased with temperature, as expected, and the oscillatory period increased monotonically with cell doubling time (Fig. 2d). The oscillator also functioned in minimal A medium with 2 g l^{-1} glucose (Fig. 2c, d). Although the cell doubling time in minimal medium was significantly longer than in LB-Miller formulation lysogeny broth (LB) (80–90 min versus 22–24 min at 37 °C), the period in the minimal medium was very similar to that in LB (Fig. 2c, d). This result, together with the strong dependence of the period on IPTG and arabinose concentration (at constant cellular doubling times), demonstrates that the synthetic oscillator is not strongly coupled to the cell cycle. The similar dependence of the period and the doubling time on the temperature seems to be due to the thermodynamic change of the rate constants affecting all cellular processes.

The oscillator was constructed according to design principles determined from previous theoretical work[1]. However, we found that this original model failed to describe two important aspects of the experiments. First, the model could not describe the observed functional dependence of the period on inducer levels. Second, and perhaps most importantly, because careful parameter tuning was necessary for oscillations in the original model, it was not able to describe the robust behaviour demonstrated in the experiments. This suggests that only a small region of inducer space should support oscillations, in contrast to the robust behaviour demonstrated in the experiments. These shortcomings forced a re-evaluation of the derivation of the oscillator equations, and led to a new computational model that more accurately described the experimental observations. The new model incorporates the same coupled positive and negative feedback architecture, but includes details that were omitted from the previous model. In particular, we found that directly modelling processes such as protein–DNA binding, multimerization, translation, DNA looping, enzymatic degradation and protein folding greatly increased the accuracy of the model. The result is a computational model that is very robust to parameter variations and correctly describes the dynamics of the oscillator for a large range of IPTG and arabinose concentrations (see Box 1 and Supplementary Information).

In examining our refined model, we discovered another region in parameter space that would support oscillatory behaviour. Our model predicted that a constantly activated system with repression controlled by a negative feedback loop could produce oscillations in the absence of positive feedback (Supplementary Fig. 19). It has been proposed that negative feedback gene networks can oscillate as long as there is delay in the feedback[16,17], and, although there is no explicit delay in our model, the intermediate steps of translation, protein folding and multimerization of LacI provide an effective form of delay[18] that is sufficient to support oscillations. We constructed this system (denoted JS013) in *E. coli* using a hybrid promoter, $p_{LlacO\text{-}1}$ (ref. 14), that is activated in the absence of LacI (or presence of IPTG) to drive both *lacI* and *yemGFP* expression (Fig. 3a). We observed oscillations in these cells when examined by single-cell microscopy under inducing conditions (Fig. 3b, Supplementary Fig. 5 and Supplementary Movie 11). These oscillations were not as distinct or regular as in the dual-feedback oscillator, and they did not always

Box 1 | Dynamic modelling of the dual-feedback oscillator circuit

We used standard techniques to construct both stochastic and deterministic computational models[3,25–28] based on the same underlying biochemical reactions illustrated in Fig. 4a (see Supplementary Information for full details of modelling). Although the interaction between transcription factors and the DNA is generally quite complicated to model in detail[29], we used experimental induction curves to calibrate the induction levels in the reactions describing the network (Supplementary Fig. 10). Over many oscillatory cycles, the deterministic simulations were then shown to give accurately the temporal evolution of the mode of the distributions generated by the exact stochastic simulations[24]. Representative time series for the protein concentrations obtained from the stochastic and deterministic models are depicted in Fig. 4b, c. The models are very robust in that oscillatory behaviour exists for a large range of parameter values and network details (Supplementary Information). Importantly, we found excellent quantitative agreement with the experimentally obtained period as a function of inducer levels (Fig. 4d, e).

The amplitude and period of the oscillations as a function of inducer levels can be conceptually explained using Fig. 4c. A burst begins with the basal transcription of messenger RNA from both promoters, encoding both the activator and the repressor. After a short delay (caused by, for example, translation, protein folding and multimerization), the amount of functional activator rises quicker than the amount of functional repressor, as shown in Fig. 4b. This occurs for two reasons. First, the activator gene is on a higher copy number plasmid than the repressor gene, meaning that more activator transcripts are produced than repressor transcripts. Second, assuming that transcription and translation of the monomeric forms of both proteins occur at similar rates, the activator will be more abundant because the functional tetrameric form of LacI requires twice as many monomers as does the functional dimeric form of AraC. As AraC levels rise, an activation burst in production of mRNA occurs due to the positive feedback loop. After LacI has been converted to a sufficient number of tetramers, the production of mRNA is turned off and the proteins decay enzymatically. Once all proteins have decayed, the promoters are freed of all bound regulators and the cycle begins anew. The length of the period is primarily determined by the time required for the proteins to decay. Therefore, the period is dependent on the rate of enzymatic decay and the magnitude of the activation burst. Furthermore, because the burst size depends on the induction characteristics of the promoter, it follows that the period is roughly proportional to the induction level of the promoter.

return to a dim state, consistent with the predictions of the computational model. Furthermore, the period was largely unaffected by IPTG concentration (varying less than 5% over three experimental runs from 0.6 mM to 20 mM IPTG), suggesting that the addition of the positive feedback loop serves the dual role of regularizing oscillations and allowing tunability of the period (see Supplementary Information).

In the context of synthetic biology, our findings indicate that caution must be exercised when making simplifying assumptions in the design of engineered gene circuits. We found that a full model of the system that takes into account intermediate steps such as multimerization, translation, protein folding and DNA looping is essential. The reason for this lies not only in the timescales of the system but also in the sequential timing of events. Because the intermediate steps in the production of functional protein take time, their introduction into the model creates an important form of delay[18–20]. We found that this effective delay greatly increases the robustness of our model. For instance, oscillatory activity in the model is only somewhat sensitive to the values chosen for system parameters (Supplementary Information), implying that nearly all cells should oscillate (Supplementary Table 1) despite minor stochastic variations in their intrinsic parameters. This determination of gene circuit design criteria in the present context of a fast, robust and tunable oscillator sets the stage for the design of applications such as expression schemes that are capable of circumventing cellular adaptability, centralized clocks that coordinate intracellular behaviour, and reverse-engineering platforms[21] that measure the global response of the genome to an oscillatory perturbation.

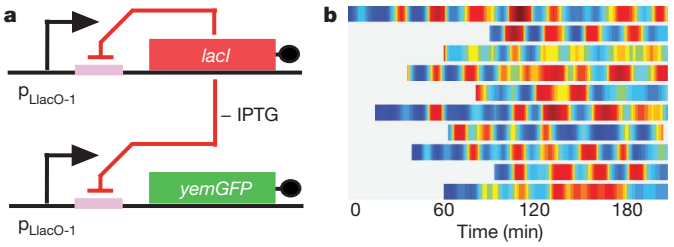

Figure 3 | An oscillator with no positive feedback loop. a, Network diagram of the negative feedback oscillator. This oscillator is similar to the dual-feedback oscillator except that the hybrid promoter $p_{LlacO-1}$ (ref. 14) gives expression of *lacI* and *yemGFP* in the absence of LacI or in the presence of IPTG without requiring an activator. **b**, Single-cell density map trajectories for cells containing this oscillator (see Supplementary Movie 11 and Supplementary Fig. 5).

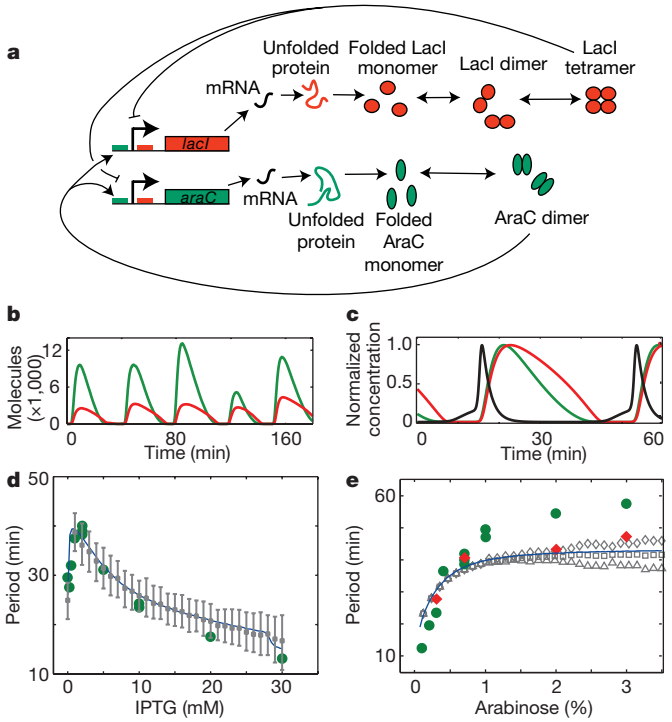

Figure 4 | Modelling the genetic oscillator. a, Intermediate processes are explicitly modelled in the refined oscillator model. **b**, **c**, Simulation results from Gillespie simulations (**b**) or deterministic modelling (**c**) at 0.7% arabinose and 2 mM IPTG. AraC dimers (green), LacI tetramers (red) and *lacI* mRNA (black) are shown. **d**, **e**, Comparison of modelling and experiment for oscillation period at 0.7% arabinose (**d**) or 2 mM IPTG (**e**). Values from deterministic modelling (blue curve), stochastic simulations (grey symbols, Supplementary Fig. 18), and microscopy (red diamonds) or flow cytometry (green circles) are shown. Lower and upper error bars in **d** represent the 16th and 84th percentiles, respectively, of the stochastic data, corresponding to ±1 s.d. for a normal distribution.

METHODS SUMMARY

The dual-feedback oscillator circuit was constructed by placing *araC*, *lacI* and *yemGFP* under the control of the hybrid $p_{lac/ara-1}$ promoter[14] in three separate transcriptional cassettes. An *ssrA* degradation tag[22] was added to each gene to decrease protein lifetime and to increase temporal resolution. These transcriptional cassettes were placed on two modular plasmids[14] and co-transformed into an Δ*araC* Δ*lacI* *E. coli* strain. The negative feedback oscillator circuit was constructed by placing *ssrA*-tagged *lacI* and *yemGFP* under the control of the $p_{LlacO-1}$ promoter[14] in two separate transcriptional cassettes, which were incorporated onto two modular plasmids and co-transformed into a Δ*lacI* strain. Cells were

grown either in LB medium or in minimal A medium with $2\,g\,l^{-1}$ glucose. Oscillations were induced using arabinose (0.1–3%) and IPTG (0–30 mM). Single-cell microscopic data were collected by loading induced cells into polydimethylsiloxane-based microfluidic platforms that constrained the cells to a monolayer while supplying them with nutrients[23], and then providing a constant source of medium and inducers and imaging GFP fluorescence every 2–3 min for at least 4–6 h. These data were further analysed using ImageJ and custom-written Matlab scripts to extract single-cell fluorescence trajectories. Flow cytometry was performed either by taking samples from a continuously grown and serially diluted culture or by growing multiple cultures in parallel for varying durations. In either case, samples were read directly from their growth medium and low-scatter noise was removed by thresholding. Flow cytometry oscillatory periods were defined as the time elapsed between the first and second fluorescence peaks. Details of the models discussed are presented in Supplementary Information. Stochastic simulations were performed using Gillespie's algorithm[24], and deterministic simulations were performed using custom Matlab scripts.

Full Methods and any associated references are available in the online version of the paper at www.nature.com/nature.

Received 9 July; accepted 5 September 2008.
Published online 29 October 2008.

1. Hasty, J., Dolnik, M., Rottschäfer, V. & Collins, J. J. Synthetic gene network for entraining and amplifying cellular oscillations. *Phys. Rev. Lett.* **88,** 148101 (2002).
2. Hasty, J., McMillen, D. & Collins, J. J. Engineered gene circuits. *Nature* **420,** 224–230 (2002).
3. Tyson, J., Chen, K. & Novak, B. Sniffers, buzzers, toggles and blinkers: dynamics of regulatory and signaling pathways in the cell. *Curr. Opin. Cell Biol.* **15,** 221–231 (2003).
4. Sprinzak, D. & Elowitz, M. B. Reconstruction of genetic circuits. *Nature* **438,** 443–448 (2005).
5. Endy, D. Foundations for engineering biology. *Nature* **438,** 449–453 (2005).
6. Andrianantoandro, E., Basu, S., Karig, D. K. & Weiss, R. Synthetic biology: new engineering rules for an emerging discipline. *Mol. Syst. Biol.* **2,** 2006.0028 (2006).
7. Gardner, T. S., Cantor, C. R. & Collins, J. J. Construction of a genetic toggle switch in *Escherichia coli*. *Nature* **403,** 339–342 (2000).
8. Elowitz, M. B. & Leibler, S. A synthetic oscillatory network of transcriptional regulators. *Nature* **403,** 335–338 (2000).
9. Atkinson, M. R., Savageau, M. A., Myers, J. T. & Ninfa, A. J. Development of genetic circuitry exhibiting toggle switch or oscillatory behavior in *Escherichia coli*. *Cell* **113,** 597–607 (2003).
10. Fung, E. *et al.* A synthetic gene-metabolic oscillator. *Nature* **435,** 118–122 (2005).
11. Kobayashi, H. *et al.* Programmable cells: interfacing natural and engineered gene networks. *Proc. Natl Acad. Sci. USA* **101,** 8414–8419 (2004).
12. You, L., Cox, R. S., Weiss, R. & Arnold, F. H. Programmed population control by cell-cell communication and regulated killing. *Nature* **428,** 868–871 (2004).
13. Barkai, N. & Leiber, S. Circadian clocks limited by noise. *Nature* **403,** 267–268 (2000).
14. Lutz, R. & Bujard, H. Independent and tight regulation of transcriptional units in *Escherichia coli* via the LacR/O, the TetR/O and AraC/I_1-I_2 regulatory elements. *Nucleic Acids Res.* **25,** 1203–1210 (1997).
15. Lee, S. K. *et al.* Directed evolution of AraC for improved compatibility of arabinose- and lactose-inducible promoters. *Appl. Environ. Microbiol.* **73,** 5711–5715 (2007).
16. Bliss, R. D., Painter, P. R. & Marr, A. G. Role of feedback inhibition in stabilizing the classical operon. *J. Theor. Biol.* **97,** 177–193 (1982).
17. Bratsun, D., Volfson, D., Tsimring, L. S. & Hasty, J. Delay-induced stochastic oscillations in gene regulation. *Proc. Natl Acad. Sci. USA* **102,** 14593–14598 (2005).
18. Rateitschak, K. & Wolkenhauer, O. Intracellular delay limits cyclic changes in gene expression. *Math. Biosci.* **205,** 163–179 (2007).
19. Mackey, M. & Glass, L. Oscillation and chaos in physiological control systems. *Science* **197,** 287–289 (1977).
20. Jaeger, J. & Reinitz, J. On the dynamic nature of positional information. *Bioessays* **28,** 1102–1111 (2006).
21. Faith, J. *et al.* Large-scale mapping and validation of *Escherichia coli* transcriptional regulation from a compendium of expression profiles. *PLoS Biol.* **5,** e8 (2007).
22. Andersen, J. B. *et al.* New unstable variants of green fluorescent protein for studies of transient gene expression in bacteria. *Appl. Environ. Microbiol.* **64,** 2240–2246 (1998).
23. Cookson, S., Ostroff, N., Pang, W. L., Volfson, D. & Hasty, J. Monitoring dynamics of single-cell gene expression over multiple cell cycles. *Mol. Syst. Biol.* **1,** 2005.0024 (2005).
24. Gillespie, D. T. Exact stochastic simulation of coupled chemical-reactions. *J. Phys. Chem.* **81,** 2340–2361 (1977).
25. Hasty, J. *et al.* Computational studies of gene regulatory networks: in numero molecular biology. *Nature Rev. Genet.* **2,** 268–279 (2001).
26. Ozbudak, E., Thattai, M., Lim, H., Shraiman, B. & van Oudenaarden, A. Multistability in the lactose utilization network of *Escherichia coli*. *Nature* **427,** 737–740 (2004).
27. Wang, X., Hao, N., Dohlman, H. & Elston, T. Bistability, stochasticity, and oscillations in the mitogen-activated protein kinase cascade. *Biophys. J.* **90,** 1961–1978 (2006).
28. Bennett, M. *et al.* Metabolic gene regulation in a dynamically changing environment. *Nature* **454,** 1119–1122 (2008).
29. Gerland, U., Moroz, J. & Hwa, T. Physical constraints and functional characteristics of transcription factor-DNA interaction. *Proc. Natl Acad. Sci. USA* **99,** 12015–12020 (2002).

Supplementary Information is linked to the online version of the paper at www.nature.com/nature.

Acknowledgements We thank H. Bujard, C. Yang, and Z. Zhang for gifts of reagents, and D. Volfson and M. Simpson for discussions. This work was supported by grants from the National Institutes of Health (GM69811-01) and the US Department of Defense.

Author Contributions J.S. and J.H. designed the oscillator circuits, and J.S. constructed the circuits. S.C. performed the microscopy experiments, and J.S. and S.C. performed the flow cytometry experiments. S.C., L.S.T. and J.H. performed the single-cell data analysis. M.R.B., W.H.M. and L.S.T. performed the computational modelling. All authors wrote the manuscript.

Author Information Reprints and permissions information is available at www.nature.com/reprints. Correspondence and requests for materials should be addressed to J.H. (hasty@bioeng.ucsd.edu).

METHODS

Oscillator plasmid and strain construction. The oscillator components *araC* and *lacI* and a fluorescent reporter protein (*yemGFP*) were tagged with carboxy-terminal TSAANDENYALAA *ssrA* tags[22]. *yemGFP* contains F64L/S65T/A206K mutations. These tagged genes were then cloned into pZ modular plasmids under the transcriptional control of the $p_{lac/ara-1}$ hybrid promoter[14] to form three co-regulated transcriptional modules with identical promoters, ribosome-binding sequences and downstream terminators. The $p_{lac/ara-1}$ promoter is activated by AraC in the presence of arabinose and repressed by LacI in the absence of IPTG. The activator *araC* module and the reporter *yemGFP* module were placed on a ColE1 plasmid, and the repressor module was placed on a p15A plasmid. All PCR-amplified sections and sequence junctions were confirmed by sequencing. (See Supplementary Fig. 1.) An Δ*araC* Δ*lacI* strain was constructed by P1*vir* phage transduction between Δ*araC* and Δ*lacI* strains. The two plasmids described above were co-transformed into this strain to construct the dual-feedback oscillator strain.

To construct the negative feedback oscillator strain, the hybrid promoter $p_{LlacO-1}$ (ref. 14) was used to regulate expression of *lacI* and *yemGFP*. This promoter is repressed by LacI in the absence of IPTG. Both genes were tagged with *ssrA* tags as described above. Two transcriptional modules containing $p_{LlacO-1}$ and *lacI* or *yemGFP* were constructed as above. The repressor module was placed on a p15A plasmid and the reporter module was placed on a ColE1 plasmid. These were then co-transformed into a Δ*lacI* strain.

Microscopy. We examined cells with single-cell time-lapse fluorescence microscopy using microfluidic devices designed to support growth of a monolayer of *E. coli* cells under constant nutrient flow (Supplementary Fig. 2). The design of the microfluidic device used in all microscopy experiments was adapted from the Tesla microchemostat design[23] for use with *Saccharomyces cerevisiae*. Modifications made to support imaging monolayers of *E. coli* included lowering the cell chamber height to match the cylindrical diameter of K-12 MG 1655 cells, lowering the delivery channel height to maintain equivalent flow splitting between the cell chamber and the bypass channel, and dividing the cell trapping region into three channels for simultaneous observation of isolated colonies (Supplementary Fig. 2a, b). For on-chip induction experiments, we used a variant of this device that incorporated a laminar boundary media switch into the design[30] and supported cell growth for several generations in non-inducing media before induction and imaging (Supplementary Fig. 2c, d).

In each experiment, a microfluidic device was mounted to the stage and wetted using a solution of 0.1% Tween 20 surfactant in the appropriate growth medium. For optimal *E. coli* growth, the chip temperature was typically maintained at 37 °C by flowing heated water through deep thermal channels fabricated into the device. Cells that had been passed from an overnight culture into inducing media approximately 3–4 h earlier were loaded into the device from the cell port by directing high flow both from the cell port and from the media port to the waste port. On trapping a single cell in each channel, flow past the cell chamber was reversed and slowed to 1–2 $\mu m\,s^{-1}$ such that fresh nutrients were delivered from the media port by means of a combination of diffusion and advection without physically disturbing the cells.

Cells grew logarithmically to fill the channels over an experimental duration of ~4–6 h, while images were acquired every 2–3 min at ×100 magnification in the transmitted and fluorescent channels. Focus was maintained during image acquisition either by manual adjustment or by contrast-based autofocus algorithms. After each imaging session, fluorescence trajectories of individual cells were extracted using the WCIF ImageJ cell analysis package. For each fluorescence frame, mean values of integrated fluorescence were calculated within constant circular areas inscribed within the boundaries of all tracked cells. Long-term fluorescence trajectories were subsequently constructed by manually tracking each cell throughout the experiment.

Flow cytometry. Oscillator cells were initially characterized by flow cytometry of batch cultures to identify inducer conditions that supported oscillations. Subsequently, time-course flow cytometry was performed on growing cultures immediately after induction to follow oscillation dynamics. This time-course flow cytometry followed one of two similar protocols. In the continuous protocol, a single culture was serially diluted to maintain logarithmic growth. The culture was induced at the initial time point, and samples were removed for flow cytometry over the course of the experiment. In the aggregate protocol, an uninduced culture in logarithmic growth was aliquoted onto different inducer concentrations, and these subcultures were allowed to grow for varying lengths of time before flow cytometry. Flow cytometry was performed directly from growing cultures, and noncellular low-scatter noise was removed by thresholding. Oscillations were tracked by measuring the mean cellular fluorescence at each time point. The amplitude of the initial oscillation was usually higher than that of subsequent oscillations, presumably owing to desynchronization of the oscillations (Supplementary Fig. 8). The oscillation period was defined as the time elapsed between the first and second oscillation peaks. All flow cytometry analysis was carried out on a Becton-Dickinson FACScan.

30. Groisman, A. *et al.* A microfluidic chemostat for experiments with bacterial and yeast cells. *Nature Methods* **2**, 685–689 (2005).